Phenyl argentate aggregates [AgnPhn+1]– (n = 2–8): Models for the self-assembly of atom-precise polynuclear organometallics

Steven Daly, Sebastian Weske, Antonija Mravak, Marjan Krstić, Alexander Kulesza, Rodolphe Antoine, Vlasta Bonačić-Koutecký, Philippe Dugourd, Konrad Koszinowski, Richard O'hair

Phenyl argentate aggregates $[Ag_nPh_{n+1}]^-$ (n = 2 - 8): models for the self-assembly of atom-precise polynuclear organometallics.

Steven Daly,[a,ξ] Sebastian Weske,[b,ξ] Antonija Mravak,[c,ξ] Marjan Krstić,[c] Alexander Kulesza,[a] Rodolphe Antoine,[a] Vlasta Bonačić-Koutecký,[c,d,e]* Philippe Dugourd,[a]* Konrad Koszinowski,[b]* Richard A. J. O'Hair[f]*

[a] Institut Lumière Matière, Université Claude Bernard Lyon 1, CNRS UMR 5306, Lyon, France. E-mail: philippe.dugourd@univ-lyon1.fr
[b] Institute of Organic and Biomolecular Chemistry, Georg-August-University Göttingen. E-mail: konrad.koszinowski@chemie.uni-goettingen.de
[c] Center of Excellence for Science and Technology - Integration of Mediterranean region (STIM), Faculty of Science, University of Split, Ruđera Boškovića 33, Split 21000, Croatia
[d] Interdisciplinary Center for Advanced Science and Technology (ICAST) at University of Split, Meštrovićevo šetalište 45, Split 21000, Croatia
[e] Chemistry Department Humboldt, University of Berlin, Brook-Taylor-Straße 2, Berlin 12489, Germany
[f] School of Chemistry and Bio21 Molecular Science and Biotechnology Institute, University of Melbourne, 30 Flemington Rd, Parkville, Victoria 3010, Australia. E-mail: rohair@unimelb.edu.au

ABSTRACT

Electrospray ionization of phenyl argentates formed by transmetallation reactions between phenyl lithium and silver cyanide provides access to the argentate aggregates, $[Ag_nPh_{n+1}]^-$, which were individually mass-selected for n = 2 – 8 in order to generate their gas-phase Ultraviolet Photodissociation (UVPD) "action" spectra over the range 304 nm to 399 nm. A strong bathochromic shift in optical spectra was observed with increasing size/n. Theoretical calculations allowed the assignment of the experimental UVPD spectra to specific isomer(s) and provided crucial insights into the transition from 2D to 3D of the metallic component with the increasing size of the complex. The

[ξ] these three authors contributed equally.

$[Ag_nPh_{n+1}]^-$ aggregates contain neither pronounced metallic cluster properties nor ligated metallic cluster features and are thus not superatom complexes. They therefore represent novel organometallic characteristics built from Ag_2Ph subunits.

INTRODUCTION

An exciting and active research frontier in the past two decades has been the development of coinage metal nanoclusters for a range of applications in chemistry, biology and physics. They continue to attract attention since they provide a link between atoms and nanoparticles,[1] and they exhibit interesting electronic properties.[2] Polynuclear coinage metal organometallic aggregates have received less attention, even though they have been implicated as multi-metallic catalysts in organic transformations[3] and can exhibit interesting photophysical properties (e.g. luminescence).[4] These are exemplified by copper and silver aryls, which play important roles in organic synthesis, either as stoichiometric reagents or as reactive intermediates in catalytic cycles.[5-10] The parent, insoluble phenyl silver, first reported by Krause and Schmitz in 1919,[11] was hypothesized by Hofstee et al in 1979 to adopt a polymeric chain like structure in which each phenyl group bridges between two silver atoms in an ipso fashion (Scheme 1A).[12] More than two decades later, the first examples of related infinite chains were reported from X-ray crystallographic studies[13,14] on perfluoro phenyl silver coordinated to nitrile solvent molecules (Scheme 1B).[15,16] More recently AgC_6F_5 has been shown to adopt a zig-zag polymeric chain structure (cf Scheme 1A).[17] Other X-ray crystallographic studies on silver aryls have revealed diverse structures ranging from singly coordinated mononuclear neutral complexes,[18] doubly coordinated mononuclear neutral[19] and "ate" complexes[20] (Scheme 1C) to various aggregates, which typically involve an aryl group bridging between two metal centers including dimers (Scheme 1D),[21] contact ion pair "ates" (Scheme 1E),[22] neutral tetramers with auxiliary ligands (Scheme 1F),[23] neutral tetramers without auxiliary ligands (Scheme 1G),[24-26] "ate" hetero pentamers (Scheme 1H).[27] The diverse structures of these solid state materials share a common $PhAg_2$ subunit that involves two-electron three-center bonding (Scheme 1I) with contribution **9a** involving the

combination of the C(sp^2) molecular orbital of the bridging aryl group with a mutually bonding combination of Ag orbitals.[28,29]

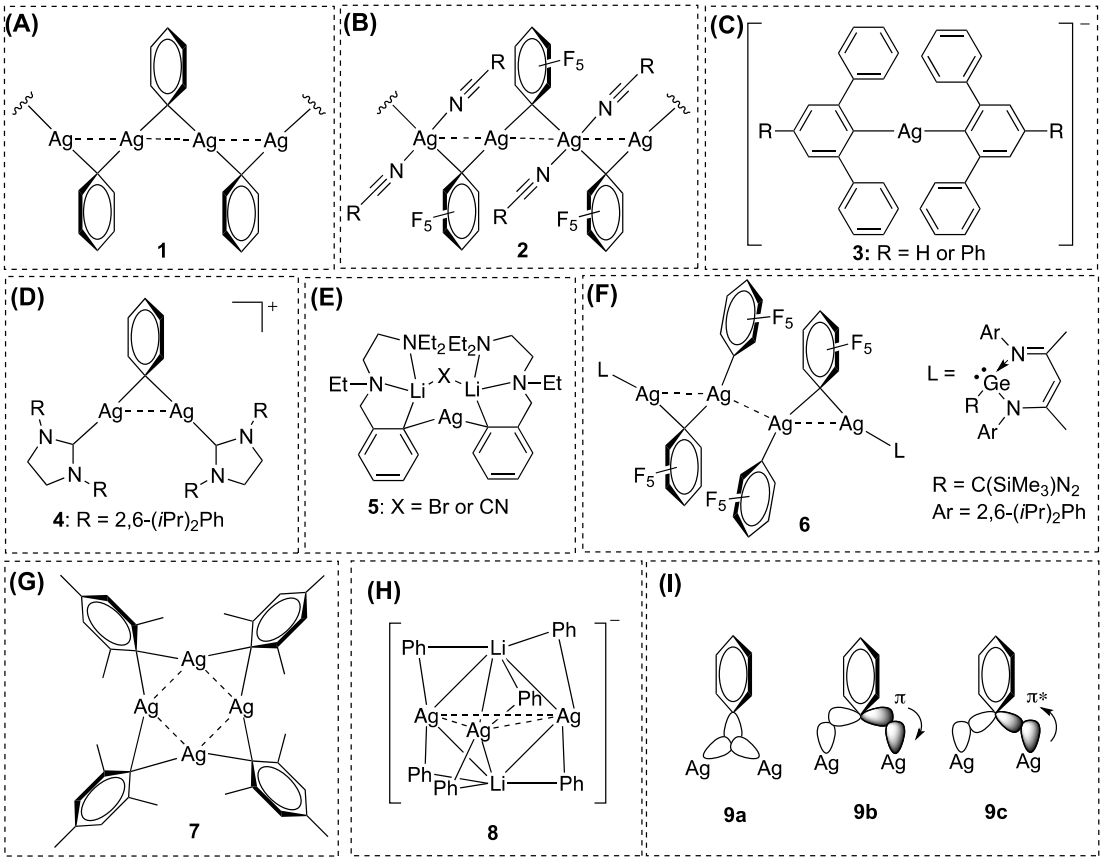

Scheme 1: Structures of silver aryls: **(A)** polymeric chain structure of phenyl silver; **(B)** polymeric chain structure of perfluoro phenyl silver coordinated to nitrile solvent molecules; **(C)** mononuclear argentates;[20] **(D)** ligated cationic dimers;[21] **(E)** contact ion pair "ate" complex;[22] **(F)** tetramer with auxiliary ligand[23]; **(G)** tetramer without auxiliary ligand[24-27]; **(H)** pentamer[28]; **(I)** orbital description of two-electron three-center bonding.[29,30]

The powerful marriage of theory and gas-phase experiments employing mass-spectrometry (MS) based methods has been used to examine the structures and reactivity of a wide range of metal clusters and aggregates.[31-33] Given the diverse range of structures of silver aryls (Scheme 1), we have a continued interest in exploring these systems in the gas phase to establish what other structures might be possible as potential targets for new materials. The interplay of mass spectrometry, laser Ultraviolet Photodissociation (UVPD) "action" spectroscopy, and density functional theory (DFT) calculations confirmed that $[AgPh_2]^-$ adopts a linear structure related to **3** (Scheme 1),[34]

while $PhAg_2^+$ contains the same motif found in **4**, where a phenyl bridges two Ag centers.[35] These phenyl silver complexes were formed in the gas phase via collision-induced dissociation (CID) decarboxylation reactions of silver benzoate precursors generated via electrospray ionization (ESI),[36] which potentially limits the numbers of such complexes that can be formed. While CID of silver tetraphenylborate aggregates generates related phenyl silver aggregates, many of these retain tetraphenyl borate ligands, adding structural complexity.[37]

Given that ESI-MS of organocuprate solutions generates aggregates,[38,39] we were encouraged to explore such an approach to generate anionic phenyl silver aggregates. Here we report the first ESI-MS studies on phenyl argentates formed by transmetallation reactions between phenyl lithium and silver cyanide, which provides access to the argentate aggregates, $[Ag_nPh_{n+1}]^-$. We focus on these anionic argentates because positive-ion mode ESI-MS of the same sample solutions affords only a limited number of organometallic cations, all of which contain not only silver, but also lithium (e.g., $[Li_2AgPh_2(THF)_2]^+$, THF = tetrahydrofuran).[40] Due to their increased complexity and their smaller number, these heteronuclear cations do not lend themselves well for the systematic analysis of aggregation effects in organometallic oligomers. The $[Ag_nPh_{n+1}]^-$ complexes where n = 2 – 8 were individually mass-selected in order to generate their UVPD spectra. Theoretical calculations were key to determining their structural and optical properties, thereby allowing the assignment of the experimental UVPD spectra to specific isomer(s). The two key questions we wish to address are: (1) At what size is there a transition from 2D to 3D for the metallic component of the aggregate? (2) Are these novel organometallic complexes built from Ag_2Ph subunits (Scheme 1I)?

EXPERIMENTAL AND THEORETICAL METHODS

Materials: All chemicals were sourced from Sigma Aldrich and used without further purification. They were: anhydrous and inhibitor free THF (≥ 99.9%); AgCN (99%); and phenyl lithium (1.9M in dibutyl ether).

Preparation of phenyl argentates: Silver cyanide (83.7 mg, 0.625 mmol, 1 equiv.) was added to a 10 mL Schlenk flask. After repeatedly evacuating and flushing with argon, the flask was heated under vacuum for 1 h. After cooling to room temperature, 5 mL of anhydrous THF was added under argon. Then, the flask was cooled down to −78 °C. To this stirred suspension was added a solution of phenyl lithium (0.66 mL of a 1.9 M solution in dibutyl ether, 1.25 mmol, 2 equiv.). After stirring at −78 °C for 25 min, the solution was diluted to a concentration of 10 mM, transferred into a gas tight syringe and injected into the ESI source of the mass spectrometer.

Mass spectrometry and UVPD experiments.

The phenyl argentate solution prepared above was introduced into a modified quadrupole linear ion trap mass spectrometer (LTQ, Thermo Fisher Scientific, San Jose, CA, USA) via ESI using a syringe pump set to a flow rate of 1 mL hr^{-1}. The typical ESI conditions used were: spray voltage, 3.4 - 3.9 kV, capillary temperature, 60°C, nitrogen sheath gas pressure, 8 - 10 (arbitrary units). Standard CID experiments were carried out by mass selecting the precursor ion and subjecting it to multicollision conditions with the helium bath gas using an activation time of 10 ms and a Q of 0.15, and choosing a normalised collision energy (NCE) such that some of the precursor ion remained.

The modification to the mass spectrometer consists of the installation of a quartz window fitted on the rear of the MS chamber to allow coupling of the laser with the linear ion trap.[41,42] The laser used was a nanosecond frequency-doubled tuneable Horizon OPO (Optical Parametric Oscillator) laser pumped by a SureliteTM II Nd:YAG laser (both from Continuum, Santa Clara, CA, USA). The repetition rate of the laser was 10 Hz with pulse widths of 5 ns. The laser beam passed through a mechanical shutter electronically synchronized with the mass spectrometer, after which it was focused with a 1000 mm lens into the linear trap on axis. The laser power was monitored with a power meter located just before the injection in the ion trap. The mechanical shutter was used to synchronize the laser irradiation with the trapping of the ions. To perform laser irradiation with a single laser pulse, we added in the ion trap radio frequency (RF) sequence an MS^n step with an activation amplitude of 0% and a reaction time of 100 ms, during which the shutter located on the laser beam was opened. The activation q value was set to 0.20.

For action spectroscopy, mass spectra were recorded after laser irradiation as a function of the laser wavelength as described in detail elsewhere.[43] At each laser wavelength from 304 nm to 399 nm (with a 0.1 nm step and 1 second dwell), a laser-normalized yield of photo-fragmentation was deduced from the mass spectrum through eq. 1:

$$\sigma = \log((precursor + products)/precursor)/ \Phi \quad (1)$$

where Φ is the laser fluence, *precursor* is the intensity of the precursor ion, and *products* represents the intensity of all the product ion peaks. Optical action spectra were obtained by plotting the normalized yield of photo-fragmentation as a function of the laser wavelength.

Theory

Structural and optical properties of the complexes were determined using density functional theory (DFT) and its time-dependent DFT (TDDFT) counterpart as implemented in the Gaussian09 suite of software (Revision D.01).[44] Structural optimization was carried out using the hybrid B3LYP[45-47] functional with def2-TZVP[48] atomic orbital basis, and Grimme's dispersion (GD3)[49] correction. Relativistic effective core[50] potential was employed for Ag atoms. An extensive search for the lowest energy structures was performed including simulated annealing. The absorption spectra at T = 0 K were obtained for the optimized geometries using TDDFT with PBE0[51,52] functional and def2-TZVP basis set with 30 electronic states being calculated. The plots cover the range between 300 and 400 nm. For determination of absorption spectra for $[Ag_6Ph_7]^-$ and $[Ag_8Ph_9]^-$, the thermal ensemble of structures at T = 300 K obtained from constant temperature Molecular Dynamics (MD) based on AM1[53] was used. The structures along MD trajectories which were used for thermal ensemble are shown in Figures S5 and S6.

RESULTS AND DISCUSSIONS:

ESI-MS on reaction mixture of silver cyanide and phenyl lithium

Negative ion ESI of the phenyl argentate solution prepared as described in the experimental section gave a rich mass spectrum (Figure 1) showing a range of silver containing anions which were readily identified by their unique isotopic signatures as well as their *m/z* values (which are listed for the most abundant peak in the isotope pattern throughout this work). Oligomers $[Ag_nPh_{n+1}]^-$ ranging from n = 2 to 8 were observed with sufficient abundance for UVPD studies. The formation of these types of well-defined even-electron oligomers is reminiscent of early studies of alkali metal halides cluster anions,[54] as well as the copper chloride cluster anions $[Cu_nCl_{n+1}]^-$.[55] Noteworthy is the lack of stoichiometries that are subvalent in silver, which contrasts with silver iodide clusters anions of the type $[Ag_nI]^-$ previously observed using other methods.[56]

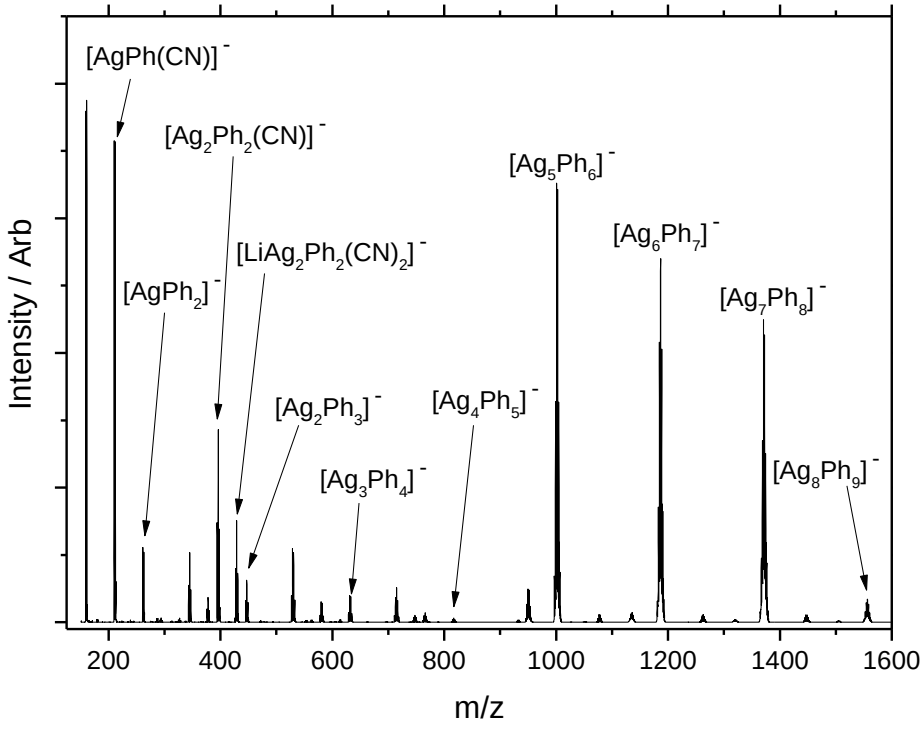

Figure S1. ESI-MS of a 10mM THF solution of the reaction mixture of PhLi and AgCN. The anions observed include (*m/z* values are for the most abundant peak in the isotope cluster): $[Ag(CN)_2]^-$ (*m/z* 159); $[AgPh(CN)]^-$ (*m/z* 210); $[AgPh_2]^-$ (*m/z* 261); $[Ag_2Ph_2(CN)]^-$ (*m/z* 396); $[LiAg_2Ph_2(CN)_2]^-$ (*m/z* 429); $[Ag_2Ph_3]^-$ (*m/z* 447); $[Ag_3Ph_4]^-$ (*m/z* 631); $[Ag_4Ph_5]^-$ (*m/z* 817); $[Ag_5Ph_6]^-$ (*m/z* 1001); $[Ag_6Ph_7]^-$ (*m/z* 1187); $[Ag_7Ph_8]^-$ (*m/z* 1371) and $[Ag_8Ph_9]^-$ (*m/z* 1557).

Size dependent structural and optical properties of organometallic aggregates, $[Ag_nPh_{n+1}]^-$ (n = 2-8).

Each of the anions $[Ag_nPh_{n+1}]^-$ (n = 2 – 8) formed via ESI were mass selected and their UVPD spectra were measured. Mass spectra are shown in Figures S1 and S2 and the fragmentation channels are discussed in more detail in the SI. The fragmentation channels observed were loss of signal due to electron loss via photodetachment (eq. 2) and losses of AgPh neutral aggregates (eq. 3). The latter are also observed under collision-induced dissociation (CID) conditions. No electron detachment was observed above 300 nm, but was observed at 260 nm for the smaller aggregates (n = 2 – 5). In contrast, it was significantly lower for n = 6 - 7.

Figure 2 highlights the similarities between CID and LID fragmentation channels for $[Ag_7Ph_8]^-$ as well as the unique UVPD fragmentation channels corresponding to losses of phenyl radicals (eq. 3) that are observed for the larger aggregates (n = 5, 7 and 8). The loss of phenyl radicals gives rise to the aggregates $[Ag_7Ph_7]^-$ and $[Ag_7Ph_6]^-$ that are subvalent in silver. Their CID spectra are given in Figures 2C and 2D reveal a richer set of fragmentation chemistry than $[Ag_7Ph_8]^-$ (Figure 2A).

$$[Ag_nPh_{n+1}]^- \rightarrow [Ag_nPh_{n+1}]^{\bullet} + e^- \quad (2)$$

$$[Ag_nPh_{n+1}]^- \rightarrow [Ag_{n-m}Ph_{n+1-m}]^- + [AgPh]_m \quad (3)$$

$$[Ag_nPh_{n+1}]^- \rightarrow [Ag_nPh_n]^- + Ph^{\bullet} \quad (4)$$

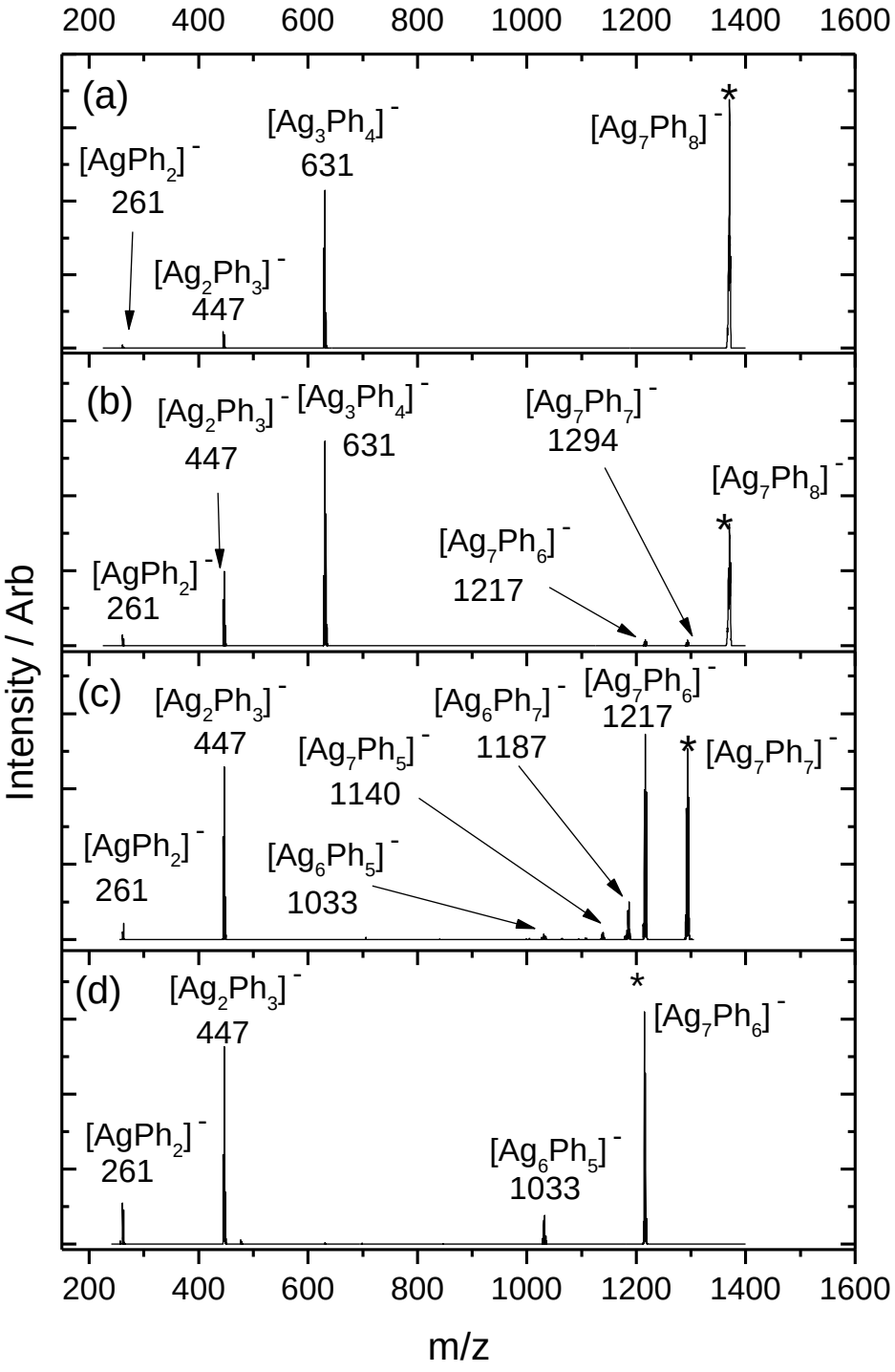

Figure 2: Comparison of the gas-phase fragmentation reactions of $[Ag_7Ph_x]^-$: (a) CID of $[Ag_7Ph_8]^-$ (*m/z* 1371, NCE = 5%); (b) LID of $[Ag_7Ph_8]^-$ (*m/z* 1371, 260 nm with an irradiation time of 100ms); (c) MS^3 CID of $[Ag_7Ph_7]^-$ formed in Figure 2(b), (*m/z* 1294, NCE = 10%); (d) MS^3 CID of $[Ag_7Ph_6]^-$ formed in Figure 2(b), (*m/z* 1217, NCE = 10%). A * represents the mass selected precursor ion. All CID experiments were carried out with an activation time of 10 ms using a Q of 0.15, with the NCE used given for each ion.

The action spectra taken between 304 and 399 nm for $[Ag_nPh_{n+1}]^-$ are given in Figure S3 and all exhibit shoulders at ~305 - 310 nm. For the anions $[Ag_6Ph_7]^-$, $[Ag_7Ph_8]^-$ and $[Ag_8Ph_9]^-$ a new band centered at ~360 nm appears.

In order to assign these features to specific isomers, we turned to detailed DFT calculations. The structural properties of the aggregates have been determined by DFT approach and corresponding absorption spectra were calculated using TDDFT method. This allowed for the structural assignment of the experimental UVPD spectra and determination of building blocks for different sizes of organometallic complexes. Regarding the structural properties shown in Figure 3, two classes with 2D and 3D metallic components have been identified. Within the 2D class of structures, in addition to Ag_2Ph subunits, AgPh was identified as a terminating unit. This is the case for the lowest energy structures of $[Ag_nPh_{n+1}]^-$ with n = 2 - 4, where there are not enough silver atoms to form compact 3D structures. The described class of structures represents also higher energy isomers for n = 4 - 8. Interestingly, the lowest energy structures for $[Ag_5Ph_6]^-$ shows a transition to the compact 3D metallic component containing Ag_2Ph subunits and the most stable structure is directly related to structures determined via X-ray crystallography (**8** [22] in Scheme 1 and $[Cu_5Ph_6]^-$ [39]). Thus, for n = 5 - 8 these 3D metallic component class of structures are energetically favourable.

As reported already, for organometallic complexes dispersion interaction plays significant role in structural stability.[57,58] In order to understand the origin of the stability of observed 3D structures (n = 5 - 8), we applied Grimme dispersion correction (GD3)[48] during DFT structural minimization of each 3D and 2D complex. Contribution of the dispersion term to the total energy of the structures in minimum is reported in the Table S1. Results clearly demonstrate that in all cases the compact structures had the larger GD3 correction and for bigger 3D complexes (n = 5 - 8) the difference is more pronounced compared to the 2D counterparts. In those 3D compact structures organic parts having π electrons are closer to each other accounting for attractive dispersion interaction between subunits which contributes to the overall stability. This observation is fully in agreement with our experimental results and previously reported studies on organometallic complexes. [57,58] DFT calculations on the gas-phase IR spectra

for the lowest energy 2D and 3D isomers of $[Ag_4Ph_5]^-$, $[Ag_7Ph_7]^-$ and $[Ag_8Ph_9]^-$ show dominant features associated with the C-H vibrations of the phenyl rings (data not shown). The small differences in the other minor features mean that IR spectroscopy is not likely to allows isomer distinction for this class of aggregates. Recent work on related organocuprates suggest that ion-mobility might provide isomer differentiation.[59]

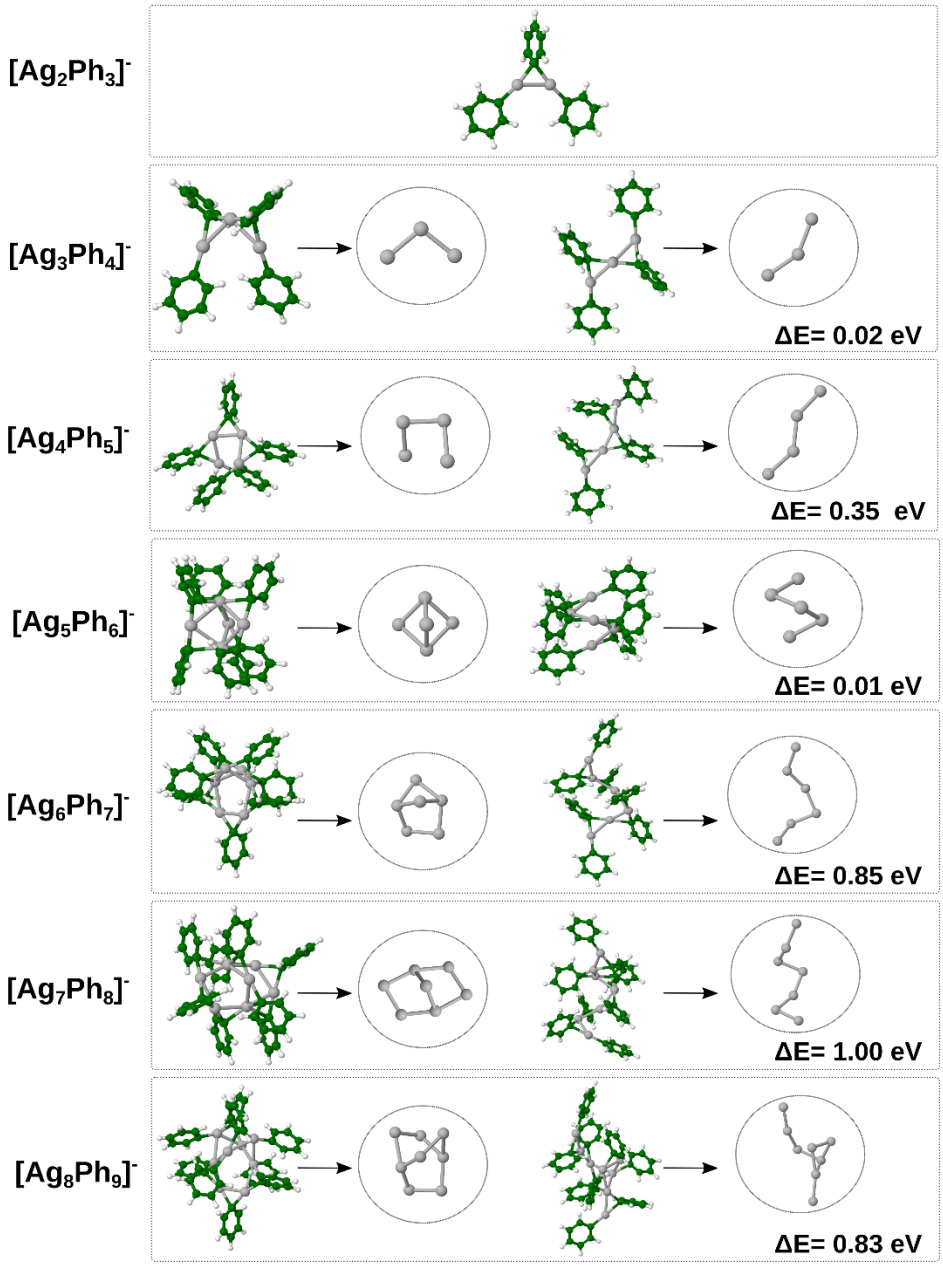

Figure 3. Optimized DFT structures of two classes of structural isomers of $[Ag_nPh_{n+1}]^-$, n = 2 - 8 together with metallic components. The 3D compact structural isomers are shown at the left, while the 2D more open structural isomers are shown at

the right. ΔE labels show the energy difference between two classes of structural isomers. The lines connecting the silver atoms represent distances within the range of 2.8 Å to 3.5 Å and are used to guide the eye for the metallic components.

The transition to the compact 3D structures is also confirmed by the comparison of calculated and experimental absorption spectra shown in Figure 4. There is an overall difference between absorption features of complexes with n = 2-4 and n = 5-8. A red shift for the lowest excited states for complexes with $n \geq 5$ is more pronounced for the compact class of structures. They are characterized by excitation from Ag_2Ph to metallic Ag_n subunit. Notice that in the case of $[Ag_6Ph_7]^-$ and $[Ag_8Ph_9]^-$ only a thermal ensemble of 10 structures at T=300K obtained from the constant temperature MD simulations provides absorption intensities between 320-380 nm in agreement with experimental findings (the ensemble of structures are shown in Figures S5 and S6 for $[Ag_6Ph_7]^-$ and $[Ag_8Ph_9]^-$ respectively). The calculated electron affinities show odd-even behaviour as a function of metallic component size which is significantly lower than in the case of metallic clusters (cf. Table S3). In addition, the intensities of excited states are low, which points to no delocalization of electrons and suggests that we are not dealing with ligated clusters containing metallic cores, but rather aggregates consisting of Ag_2Ph building blocks, illustrating the concept for new materials.

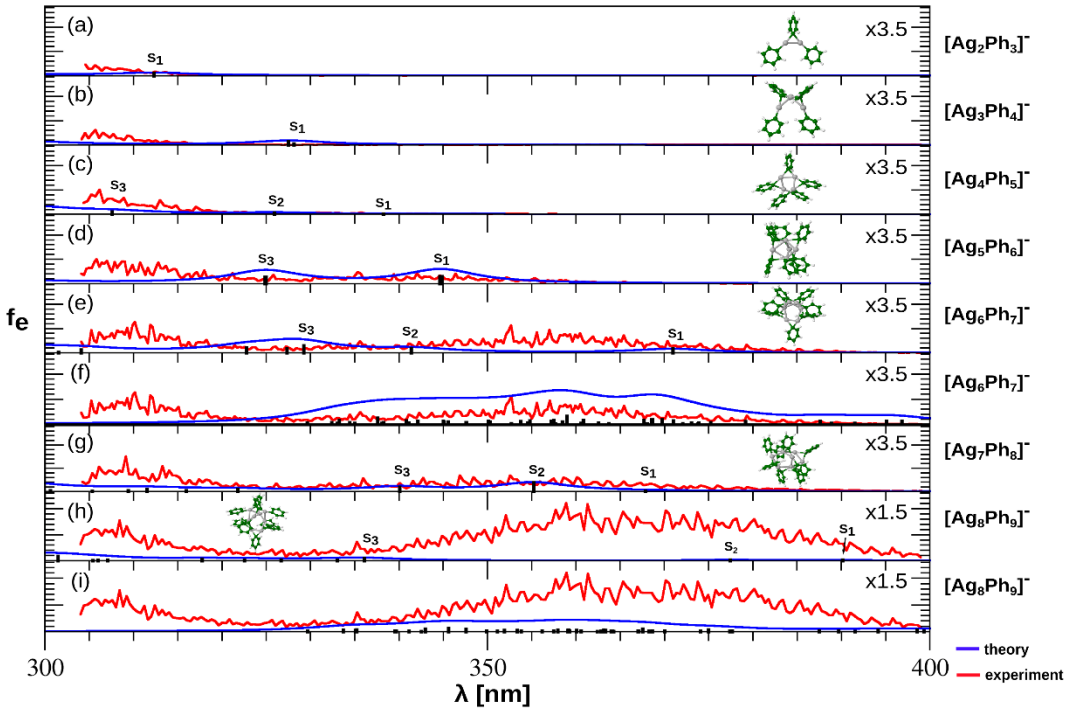

Figure 4. Comparison of experimental action spectra taken over the range 304nm to 399nm of $[Ag_nPh_{n+1}]^-$, n=2-8 with calculated absorption spectra (a)-(e), (g)-(h) for lowest energy structures using TDDFT approach (cf. Figure 1. for the structures). (f) and (i) Simulated thermally broadened absorption spectra of $[Ag_6Ph_7]^-$ and $[Ag_8Ph_9]^-$ (blue) at T=300K compared with experimental action spectrum (red). Thermal ensemble of 10 structures (containing 3D metallic subunits) at T=300K is obtained from constant temperature MD simulations (within AM1 approach) starting from the lowest energy structure. f_e represents the calculated oscillator strengths. For experimental intensities arbitrary units have been used. The scaling factors are used to visualize spectra for different species.

In fact, transition from 2D to 3D metallic component influences absorption spectra of $[Ag_5Ph_6]^-$ and the nature of excitations responsible for the first three lowest excited states, as shown in Figure 5. In the case of 2D metallic component, the AgPh contributions of end Ag atoms are present in excitations. In contrast, for 3D component contributions from Ag_2Ph remain in excitations due to compact metallic part. This is reflected in MOs on the right side of Figure 5 which illustrates that within the compact 3D structure, the excitations occur within Ag_5 bipyramid. In contrast, in the case of the 2D structure, the AgPh terminating units, as well as linear Ag_3 subunit are involved in excitations within S_1, S_2, S_3 states.

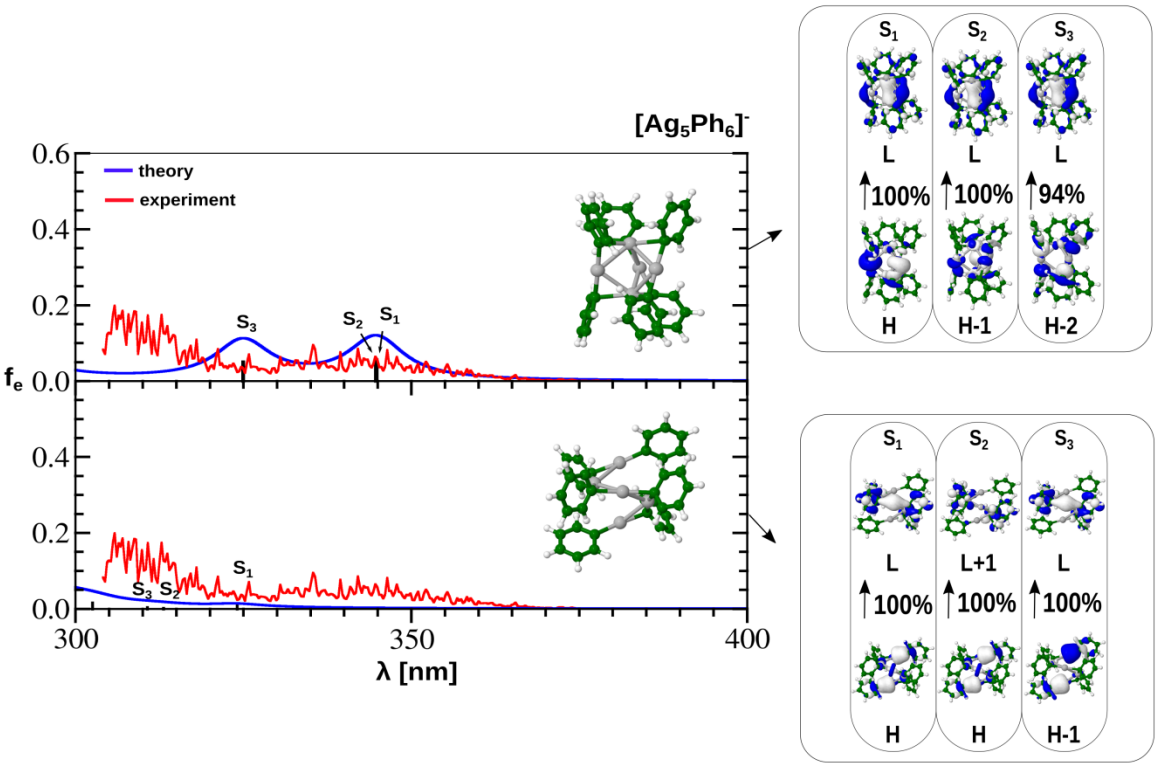

Figure 5. Comparison of experimental and DFT spectra for two classes of structures of $[Ag_5Ph_6]^-$ together with excitations among HOMO (H), HOMO-1 (H-1), HOMO-2 (H-2) to LUMO (L), LUMO+1 (L+1) responsible for the three lowest energy excited states S_1, S_2, S_3.

The transition from 2D to 3D metallic component not only influences the absorption spectrum and the nature of the excitations that leads to it, but also the experimentally observed relaxation channels. When the relaxation channels at 260 nm are examined (Table S2), structures up to $[Ag_5Ph_6]^-$ relax predominantly by electron detachment. There is a clear demarcation between $[Ag_5Ph_6]^-$ and $[Ag_6Ph_7]^-$, with the former showing 53% electron detachment yield, and the later only 4%. At the same time, the fragmentation yield increases with the size of the aggregates. This change in photophysical properties between n = 5 and n = 6 indicates a change in the nature of the optically accessed excited states, and is entirely consistent with the change from 2D to 3D structures predicted from the theory.

CONCLUSIONS

Altogether, phenyl argentate aggregates show specific structural and optical properties for organometallic complexes. A transition from 2D to 3D structures of the metallic components is evidenced and is accompanied by a strong bathochromic shift in optical spectra, useful for tuning optical properties in such argentate aggregates. They contain neither pronounced metallic cluster properties nor ligated metallic cluster features. They are not superatom complexes but rather are systems with novel organometallic characteristics. The size effect shows the formation of structures due to interaction among Ag_2Ph subunits representing building blocks of these complexes which bridges the role of metallic and organic components. Given the compact structure for $[Cu_5Ph_6]^-$ [39] similar behavior might be expected for other polynuclear organometallates. An intriguing question is whether such structures might be translated to the solid state to generate new materials. A key issue is that the anionic charge will need to be balanced by a counter cation. Previous work on translating gas-phase cations to the solid state have shown that the counter ion (in that case an anion) needs to be non-coordinating in order to not disrupt structure.[60]

SUPPLEMENTARY INFORMATION

See supplementary information for: CID and LID (260 nm) spectra and discussion of fragmentation reactions for $[Ag_nPh_{n+1}]^-$; action spectra for $[Ag_nPh_{n+1}]^-$; DFT calculated gas-phase IR spectra for $[Ag_4Ph_5]^-$, $[Ag_7Ph_7]^-$ and $[Ag_8Ph_9]^-$; DFT calculated dispersion energy correction (eV) for two classes of isomers of $[Ag_nPh_{n+1}]^-$; relative yields for electron detachment and fragmentation at 260 nm for $[Ag_nPh_{n+1}]^-$; DFT calculated electron affinity (eV) for compact structures of $[Ag_nPh_{n+1}]^-$; ensemble of structures for $[Ag_6Ph_7]^-$ and $[Ag_8Ph_9]^-$ at 300 K obtained from MD; Cartesian coordinates of relevant DFT optimized structures.

DATA AVAILABILITY STATEMENT

Data available in article or supplementary material: The data that supports the findings of this study are available within the article and its supplementary material.

ACKNOWLEDGEMENTS

R.A.J.O. and P.D. thank the Australian Research Council for financial support (DP150101388). R.A.J.O. thanks the Alexander Humboldt foundation for a senior fellowship. The research leading to these results has received funding from the European Research Council under the European Union's Seventh Framework Programme (FP7/2007-2013 Grant agreement N°320659). This research was partially supported by the project STIM-REI, Contract Number: KK.01.1.1.01.0003, funded by the European Union through the European Regional Development Fund – the Operational Programme Competitiveness and Cohesion 2014–2020 (KK.01.1.1.01). S.W. and K.K. thank the Deutsche Forschungsgemeinschaft for financial support (KO 2875/6). VBK, MK and AM acknowledge computational facilities of the HPC computer within the STIM-REI project, Doctoral study of Biophysics at University of Split as well as Prof. Miroslav Radman at MedILS and Split-Dalmatia County for support.

REFERENCES

(1) I. Chakraborty and T. Pradeep, Chem. Rev. **117**, 8208 (2017).

(2) B. Q. Yin and Z. X. Luo, Coord. Chem. Rev. **429**, 213643 (2020).

(3) J. Tanga and L. Zhao, Chem. Commun. **56**, 1915 (2020).

(4) J. M. López-de-Luzuriaga, M. Monge, and M. E. Olmos, Dalton Trans. **46**, 2046 (2017).

(5) N. Krause, *Modern organocopper chemistry*. John Wiley & Sons: Germany, 2002.

(6) Z. Rappoport and I. Marek, *The chemistry of organocopper compounds*. John Wiley & Sons: UK, 2009.

(7) A. Alexakis, J. E. Bäckvall, N. Krause, O. Pàmies, and M. Diéguez, Chem. Rev. **108**, 2796 (2008).

(8) S. R. Harutyunyan, T. den Hartog, K. Geurts, A. J. Minnaard, and B. L. Feringa, Chem. Rev. **108**, 2824 (2008).

(9) B. Breit and Y. Schmidt, Chem. Rev. **108**, 2928 (2008).

(10) J.-M. Weibel, A. Blanc, and P. Pale, Chem. Rev. **108**, 3149 (2008).

(11) E. Krause and M. Schmitz, Ber. Deutsch. Chem. Ges., **52**, 2150 (1919).

(12) H. K. Hofstee, J. Boersma, and G. J. M. Van Der Kerk, J. Organomet. Chem., **168**, 241 (1979).

(13) G. van Koten, S. L. James, and J. T. B. H. Jastrzebski, In *Comprehensive Organometallic Chemistry II*, Volume 3, pp 57-133; Pergammon, Oxford, UK, 1995.

(14) C. E. Holloway and M. Melnik, Rev. Inorg. Chem., **15**, 147 (1995).

(15) W. Tyrra and M. S. Z. Wickleder, Anorg. Allg. Chem. **628**, 1841 (2002).

(16) M. Kuprat, M. Lehmann, A. Schulz, and A. Villinger, Organometallics **29**, 1421 (2010).

(17) M. Farooq Ibad, A. Schulz, and A. Villinger, Organometallics **34**, 3893 (2015).

(18) R. Lingnau and J. Strähle, Angew. Chem. Int. Ed. Engl. **27**, 436 (1988).

(19) R. Usón, A. Laguna, A. Usón, P. G. Jones, and K. Meyer-Bäse, J. Chem. Soc. Dalton Trans. 341 (1988).

(20) C. -S. Hwang and P. P. J. Power, J. Organomet. Chem. **589**, 234 (1999).

(21) B. K. Tate, A. J. Jordan, J. Bacsa, and J. P. Sadighi, Organometallics **36**, 964 (2017).

(22) C. M. Kronenburg, J. T. Jastrzebski, J. Boersma, M. Lutz, A. L. Spek, and G. van Koten, J. Am. Chem. Soc. **124**, 11675 (2002).

(23) N. Zhao, J. Zhang, Y. Yang, H. Zhu, Y. Li, and G. Fu, Inorg. Chem. **51**, 8710 (2012).

(24) S. Gambarotta, C. Floriani, A. Chiesa-Villa, and C. A Guastini, J. Chem. Soc. Chem. Commun. 1087 (1983).

(25) E. M. Meyer, S. Gambarotta, C. Floriani, A. Chiesi-Villa, and C. Guastini, Organometallics **8**, 1067 (1989).

(26) D. A. Edwards, R. M. Harker, M. F. Mahon, and K. C. Molloy, J. Chem. Soc. Dalton Trans. 3509 (1997).

(27) H. Voelker, D. Labahn, F. M. Bohnen, R. Herbst-Irmer, H. W. Roesky, D. Stalke, and F. T. Edelmann, New J. Chem. **23**, 905 (1999).

(28) M. Y. Chiang, E. Bohlen, and R. Bau, *J. Am. Chem. Soc.* **107**, 1679 (1985).

(29) J. C. Green, M. L. Green, and G. Parkin, Chem. Commun. **48,** 11481 (2012).

(30) T. G. Gray and J. P. Sadighi, *Molecular Metal-Metal Bonds* 397, 2015.

(31) R. A. J. O'Hair and G. N. Khairallah, J. Cluster Sc., **3**, 331 (2004).

(32) Z. X. Luo, A. W. Castleman, and S. N. Khanna, Chem. Rev. **116**, 14456 (2016).

(33) S. Daly, C. M. Choi, A. Zavras, M. Krstić, F. Chirot, T. U. Connell, S. J. Williams, P. S. Donnelly, R. Antoine, A. Giuliani, V. Bonačić-Koutecký, P. Dugourd, and R. A. J. O'Hair, J. Phys. Chem. C **121**, 10719 (2017).

(34) M. I. S. Röhr, J. Petersen, C. Brunet, R. Antoine, M. Broyer, P. Dugourd, V. Bonačić-Koutecký, R. A. J. O'Hair, and R. Mitrić, J. Phys. Chem. Lett. **3**, 1197 (2012).

(35) C. Brunet, R. Antoine, M. Broyer, P. Dugourd, A. Kulesza, J. Petersen, M. I. S. Röhr, R. Mitrić, V. Bonačić-Koutecký, and R. A. J. O'Hair, J. Phys. Chem. A **115**, 9120 (2011).

(36) R. A. J. O'Hair and N. J. Rijs, Acc. Chem. Res. **48**, 329 (2015).

(37) T. Auth, K. Koszinowski, and R. A. J. O'Hair, Organometallics **39**, 25 (2020).

(38) A. Putau, M. Wilken, and K. Koszinowski, Chem. Eur. J., **19**, 10992 (2013).

(39) P. G. Edwards, R. W. Gellert, M. W. Marks, and R. Bau, J. Am. Chem. Soc. **104**, 2072 (1982).

(40) S. Weske, From Copper to Gold: Identification and Characterization of Coinage-Metal Ate Complexes by ESI Mass Spectrometry and Gas-Phase Fragmentation Experiments, PhD Thesis, University of Göttingen, 2020.

(41) V. Larraillet, R. Antoine, P. Dugourd, and J. Lemoine, Anal. Chem. **81**, 8410 (2009).

(42) R. Antoine and P. Dugourd, Visible and ultraviolet spectroscopy of gas phase protein ions, Phys. Chem. Chem. Phys. **13**, 16494 (2011).

(43) S. Daly, A. Kulesza, G. Knight, L. MacAleese, R. Antoine, and P. Dugourd, J. Phys. Chem. A, **120**, 3484 (2016).

(44) Gaussian 09, Revision D.01, M. J. Frisch, G. W. Trucks, H. B. Schlegel, G. E. Scuseria, M. A. Robb, J. R. Cheeseman, G. Scalmani, V. Barone, B. Mennucci, G. A. Petersson, H. Nakatsuji, M. Caricato, X. Li, H. P. Hratchian, A. F. Izmaylov, J. Bloino, G. Zheng, J. L. Sonnenberg, M. Hada, M. Ehara, K. Toyota, R. Fukuda, J. Hasegawa, M. Ishida, T. Nakajima, Y. Honda, O. Kitao, H. Nakai, T. Vreven, J. A. Montgomery, Jr., J. E. Peralta, F. Ogliaro, M. Bearpark, J. J. Heyd, E. Brothers, K. N. Kudin, V. N. Staroverov, R. Kobayashi, J. Normand, K. Raghavachari, A. Rendell, J. C. Burant, S. S. Iyengar, J. Tomasi, M. Cossi, N. Rega, J. M. Millam, M. Klene, J. E. Knox, J. B. Cross, V. Bakken, C. Adamo, J. Jaramillo, R. Gomperts, R. E. Stratmann, O. Yazyev, A. J. Austin, R. Cammi, C. Pomelli, J. W. Ochterski, R. L. Martin, K. Morokuma, V. G. Zakrzewski, G. A. Voth, P. Salvador, J. J. Dannenberg, S. Dapprich, A. D. Daniels, Ö. Farkas, J. B. Foresman, J. V. Ortiz, J. Cioslowski, and D. J. Fox, Gaussian, Inc., Wallingford CT, 2009.

(45) A. D. Becke, Phys. Rev. **38**, 3098 (1988).

(46) A. D. Becke, J. Chem. Phys. **98**, 5648 (1993).

(47) C. Lee, W. Yang, and R. G. Parr, Phys. Rev. B **37**, 785 (1988).

(48) F. Weigend and R. Ahlrichs, Phys. Chem. Chem. Phys. **7**, 3297 (2005).

(49) S. Grimme, J. Antony, S. Ehrlich, and H. Krieg, J. Chem. Phys. **132**, 154104 (2010).

(50) D. Andrae, U. Haeussermann, M. Dolg, H. Stoll and H. Preuss, Theor. Chim. Acta **77**, 123 (1990).

(51) C. Adamo and V. Barone, J. Chem. Phys. **110** 6158 (1999).

(52) M. Ernzerhof and G. E. Scuseria, J. Chem. Phys. **110**, 5029 (1999).

(53) M. J. S. Dewar, E. G. Zoebisch, E. F. Healy, and J. J. P. Stewart, J. Am. Chem. Soc. **107**, 3902 (1985).

(54) A. N. Alexandrova, A. I. Boldyrev, Y. J. Fu, X. Yang, X. B. Wang, L. S. Wang, J. Chem. Phys. ***121***, 5709 (2004).

(55) Z. Luo, J. C. Smith, W. H. Woodward, A. W, Castleman, J. Phys. Chem. A ***116***, 2012 (2012)

(56) C. K. Fagerquist, D. K. Sensharma, M. A. El-Sayed, J. Phys. Chem. ***95***, 9176 (1991).

(57) D. Liptrot and P. Power, Nat. Rev. Chem. **1**, 0004 (2017).

(58) J. P. Wagner and P. R. Schreiner, Angew. Chem. Int. Ed. **54**, (2015).

(59) T. Auth, M. Grabarics, M. Schlangen, K. Pagel, K. Koszinowski, Modular Ion Mobility Calibrants for Organometallic Anions Based on Tetraorganylborate Salts, Anal. Chem., manuscript under revision.

(60) I. Krossing and A. Reisinger, Coord. Chem. Rev. **250**, 2721 (2006).